PAPER • **OPEN ACCESS**

A fast helium beam diagnostic at the island divertor of W7-X for the investigation of plasma edge dynamics

To cite this article: S Hörmann *et al* 2026 *Plasma Phys. Control. Fusion* **68** 025003

Plasma Physics and Controlled Fusion

PAPER

OPEN ACCESS

RECEIVED
28 October 2025

REVISED
16 December 2025

ACCEPTED FOR PUBLICATION
13 January 2026

PUBLISHED
30 January 2026

A fast helium beam diagnostic at the island divertor of W7-X for the investigation of plasma edge dynamics

S Hörmann[1,2,*], M Griener[1], M Krychowiak[3], D Gradic[3], F B T Siddiki[3,4], M Astrain[1], E Flom[5], G Birkenmeier[1,2], A von Stechow[3], C Killer[3], F Reimold[3], S Sereda[3], T Romba[3], K J Brunner[3], J Knauer[3], U Stroth[1,2], the ASDEX Upgrade Team[6] and the W7-X Team[7]

[1] Max Planck Institute for Plasma Physics, 85748 Garching, Germany
[2] Technical University of Munich, TUM School of Natural Sciences, Physics Department, 85747 Garching, Germany
[3] Max-Planck-Institut für Plasmaphysik, 17491 Greifswald, Germany
[4] University of Wisconsin Madison, Madison, WI 53706, United States of America
[5] Thea Energy, NJ 07032 Kearny, United States of America
[6] See Zohm *et al* 2024 (https://doi.org/10.1088/1741-4326/ad249d) for the ASDEX Upgrade Team.
[7] See Grulke *et al* 2024 (https://doi.org/10.1088/1741-4326/ad2f4d) for the W7-X Team.
[*] Author to whom any correspondence should be addressed.

E-mail: sebastian.hoermann@ipp.mpg.de

Keywords: helium beam, plasma dynamics, electron density, electron temperature, island divertor, long-range correlation, Wendelstein 7-X

Abstract

Understanding and quantifying particle and energy transport at the plasma edge region is crucial for magnetic confinement fusion. For this purpose, a new polychromator system with 1 µs time resolution was installed for the thermal helium beam diagnostic in the island divertor of the stellarator Wendelstein 7-X (W7-X). The time resolution is four orders of magnitude faster than the spectrometer-based system. This allows for the first time access to turbulence-relevant time scales, enabling the investigation of plasma edge dynamics such as modes and instabilities. Their connection to averaged plasma profiles is likewise accessible with this diagnostic. Furthermore, the diagnostic system measures in two magnetically connected divertors, which enables the study of long-range correlation of fluctuations. Utilising a collisional-radiative model, the diagnostic can reconstruct fast electron density and temperature variations with an effective resolution of 10 kHz, associated with plasma modes and bursts. Additionally, it provides high temporal resolution measurements of the detachment process in the divertor. Since it simultaneously measures at an upper and lower divertor, it is the first edge diagnostic at W7-X capable of measuring the up–down asymmetry of turbulence. This article presents the design and implementation of the diagnostic as well as an analysis of the signal quality. It also looks at the influence of diagnostic gas puffs on the plasma in detail. To present the potential of the diagnostic, this work briefly shows a long-range correlation analysis of an edge mode between two divertors that are magnetically connected as well as the electron temperature and density calculation for this mode. Furthermore, a detachment process measured with high time resolution is presented.

1. Introduction

One of the key challenges for magnetic fusion devices is the control of heat and particle exhaust. To address this, most devices employ divertors, regions spatially separated from the confined plasma, where open magnetic field lines near the edge of the confined region terminate on a target. The stellarator Wendelstein 7-X (W7-X) employs the so-called *island divertor* concept [1, 2], which was first implemented in W7-AS [2, 3]. In this concept, large intrinsic magnetic islands form on low-rational magnetic surfaces at the plasma boundary. Divertor target plates intersect these islands to establish particle and energy exhaust. This creates a region of open magnetic field lines, the so-called scrape-off layer (SOL), where the island structure magnetically separates the target region from the main plasma. This spatial

separation results in a lower sputtering of the wall inside the divertor and a better density build-up in the divertor [4], which retains recycled particles and therefore lowers the impurity content in the core plasma [5].

Understanding the profiles, dynamics, and transport processes in such divertor regions, particularly in relation to the magnetic island topology, heating power, and fuelling, is essential for validating divertor performance under different conditions and for optimising the divertor concept and operational scenarios. One of the most critical parameters is the ratio of parallel to perpendicular transport, which determines the radial gradient scale lengths of temperature and density in the divertor, and therefore the local wall loads. This is especially relevant for island divertors, where the magnetic connection length can reach several 100 m, leading to a more significant influence of perpendicular transport with respect to the parallel transport than in comparable tokamaks with connection lengths of the order of 1–10 m [5, 6]. The perpendicular transport is dominated by turbulence, drifts, modes or instabilities [5], which are poorly understood. Moreover, fast processes can lead to transient peak wall loads, increasing sputtering of the plasma-facing components in a highly non-linear manner [7–9]. Such phenomena have already been observed in various tokamak regimes and it is shown that very fast high intensity events dominate the far SOL [10–12]. Despite first analyses with the multi-purpose manipulator (MPM) and simulations showing that filaments do not contribute much to radial transport in stellarators with island divertors [13], it is important to analyse different poloidal and toroidal positions, as well as other effects such as modes and bursts.

Several diagnostics are already in place to investigate the fast plasma edge dynamics at W7-X. For instance, the gas puff imaging (GPI) system at the midplane provides high-resolution observations of seeded gas emission, allowing to resolve 2D structures [14, 15]. Electric probes on the MPM enable floating potential measurements with high temporal resolution across the midplane island, enabling the study of plasma dynamics inside the island [16, 17]. Langmuir probes (LPs) installed in the divertor provide localised information on plasma parameters in front of the wall [18]. Additionally, an alkali beam (ALB) diagnostic can resolve fast electron density fluctuations across a midplane island [19, 20].

Despite this powerful set of diagnostics at W7-X, several gaps remain in our understanding of edge plasma dynamics. Firstly, fast electron temperature measurements in the SOL are limited to a few probe-based observations [13]; a continuous, high-resolution spatiotemporal T_e profile is currently lacking, though it is essential for fully capturing edge plasma dynamics. Secondly, except for the divertor LPs, all fast diagnostics focus on midplane islands, while measurements directly in the divertor region are lacking, measurements that are vital for studying wall loads and divertor-specific phenomena such as detachment. Furthermore, simultaneous high-temporal-resolution measurements of the same diagnostic at different toroidal and poloidal positions are currently missing, despite such measurements being crucial to resolve the three-dimensional (3D) nature of plasma profiles and turbulence in stellarators. This data can, for example, enable the study of up–down asymmetries and long-range toroidal correlations in fast dynamics, providing deeper insight into the nature of turbulence.

In the following, we describe the implementation of a fast helium beam diagnostic deployed at multiple locations, which offers a unique capability to locally resolve the fast structure of edge and divertor plasma dynamics in n_e and T_e with high spatiotemporal resolution. The paper is organised as follows: section 2 outlines the hardware components and the diagnostic principle. Herein, section 2.1 provides a detailed discussion of signal quality, helium puff requirements, and the influence of the diagnostic on the main plasma. Section 2.2 compares the fast helium beam diagnostic with the existing slower helium beam systems. Section 3 presents the diagnostics capabilities and briefly first analysis and results with respect to fast n_e and T_e measurements, detachment analysis, and toroidal long-range correlation studies. Finally, section 4 summarises the work.

2. Fast thermal helium beam diagnostic

The thermal helium beam diagnostic is an active spectroscopy system optimised for measurements at the plasma edge. It has already been used at several other devices, including WEST [21], TEXTOR [22], TCV [23], ASDEX Upgrade (AUG) [24, 25], RFX-mod [26], and JET [27]. With our setup we detect the emission of four helium lines: two singlet lines at 667.8 nm and 728.1 nm, and two triplet line at 706.5 nm and 587.6 nm, all originating from actively injected neutral helium. From the measured relative intensities, two line ratios can be formed: one between the two singlet lines ($I_{667.8\mathrm{nm}}/I_{728.1\mathrm{nm}}$), and one between a singlet and a triplet line ($I_{728.1\mathrm{nm}}/I_{706.5\mathrm{nm}}$). The first ratio is predominantly density-dependent, while the second one is mainly temperature-dependent [28, 29].

By comparing the measured line ratios with the ratio of the electron photon emissivity coefficient from ADAS [30] for different plasma parameters, the electron density n_e and temperature T_e can

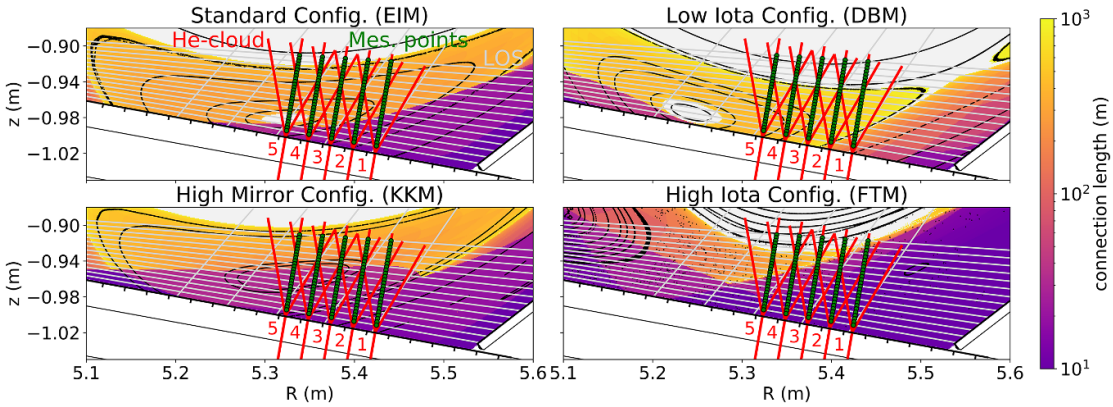

Figure 1. Schematic pictures of the helium beam system and the island region of the lower divertor in module 3 for four different magnetic configurations. The colour code gives the connection length, while the black contours represent Poincaré plots. The gas cloud of five valves with a full opening angle of 40° is plotted in red. The numbers of the different valves are written next to them. Half of the LOS are marked in grey, and the intersection point of the horizontal LOS and the central cloud axis is marked by green points.

be reconstructed [25, 28, 29]. We call this the static model, which is used in the following analysis. Compared to this, a dynamic model for W7-X is under development, but not yet implemented, which takes dynamic singlet-triplet mixing and reabsorption into account and is based on the AUG forward model, see [31] and references therein. Accounting for reabsorption of the emitted photons increases the precision of the result at high neutral helium densities, while the dynamic state mixing improves the reconstruction at low density and enables the analysis of faster processes. Furthermore, this dynamic model integrates the radiance along each line of sight (LOS) and includes, therefore, the full 3D orientation of the helium cloud and the LOS. For this model an additional line ratio ($I_{728.1\mathrm{nm}}/I_{587.6\mathrm{nm}}$) and the absolute helium line intensity at 587.6 nm is used [31]. This model assumes that the plasma is frozen and that n_e and T_e are constant along the field lines. It also assumes that the helium cloud behaves like a double Gaussian function, with its full width of half maximum corresponding to the opening angle [31, 32]. In addition to the dynamic model, the 587.6 nm line is used primarily for fast analyses for which no density and temperature reconstruction is possible. The reason is its higher emission and therefore higher signal-to-noise ratio (SNR), see section 2.1.

A helium beam diagnostic is already installed at W7-X [33]. This diagnostic allows for determining 2D temperature and density profiles [34], which were used to distinguish between two transport regimes in the island, and to estimate the $E \times B$ drift around the island [35]. This diagnostic is well suited for time-averaged profile determination, but due to the detection system based on spectrometers and CCD cameras, it has a limited temporal resolution of 25 ms. To study faster dynamics, we installed a new polychromator system, similar to the existing system at AUG, which is capable of measurements with a temporal resolution down to 1 µs by using photomultiplier tube (PMT) arrays [24, 25].

For this upgrade, the same in-vessel components and LOS as the existing helium beam system are used [33, 34], consisting of five piezoelectric valves, 32 LOS and the optical heads with the associated fibres of 140 µm core diameter. Figure 1 shows a schematic of the diagnostic in four typical configurations of W7-X. For W7-X, the standard configuration is the configuration with no currents in the planar coils and an equal current in all non-planar coils. It has an edge rotational transform of $\iota/2\pi = 5/5$ leading to a 5/5 island chain surrounding the last closed flux surface. Changing the edge rotational transform to $\iota/2\pi = 4/5$ or $\iota/2\pi = 6/5$ leading to a 4/5 and 6/5 island chain, which correspond to the low- and high-iota configuration. The high mirror configuration has the same edge rotational transform as the standard configuration, but the mirror fraction is higher [36, 37]. The black lines in figure 1 represent magnetic flux surfaces, while the colour code indicates the connection length of the field lines in the island region. With this colour map, the target shadow region (TSR) can be identified as purple area with low connection length, while the confined regions appear white due to the closed magnetic flux surfaces.

The diagnostic uses 32 LOS, shown in grey, from which 27 look in the poloidal direction and up to 5 in the z-direction. The He-beam itself is produced by one of the five piezoelectric valves embedded under the divertor plates. The resulting helium clouds, with a full opening angle of 40° [33], are marked in red. Changing between the five valves allows for varying the effective measurement locations. In the standard configuration and the high mirror configuration, the innermost valve injects helium near

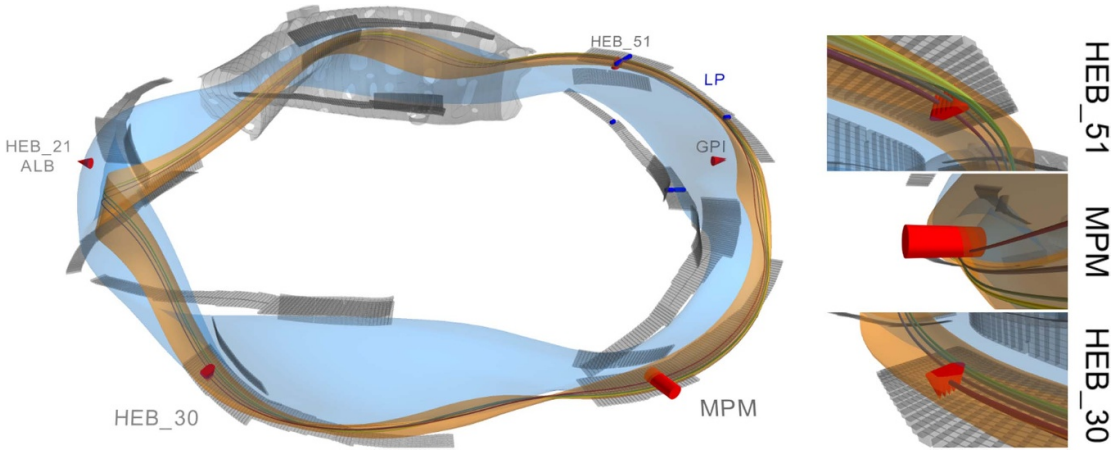

Figure 2. 3D representation of W7-X in standard configuration. In dark grey, the divertor targets are plotted, while the vessel is shown in light grey and the main plasma is plotted in blue. The island, which intersects both divertor helium beam systems (HEB_30, HEB_51) and the multi-purpose manipulator (MPM), is highlighted in orange, while the volumes observed by the diagnostics are shown in red. The other fast edge diagnostics that are not magnetically connected are also marked, including the midplane helium beam (HEB_21), gas puff imaging (GPI), the alkali beam (ALB), and the divertor Langmuir probes (LP), the latter of which is marked in dark blue. A field line starting at HEB_30 and surrounding the torus four times is shown as a thin colour-coded tube. The colour-code of the tube shows the distance along this field line, while blue/dark colours represent low length and yellow/light colours represent high length. A zoom at each magnetic connected diagnostic is shown on the right side of the picture.

the island centre, while the remaining valves are located in the direction of the TSR. For the static collisional radiative model (CRM) described above, we assume that the measurement is located at the intersection of the LOS with the centre of the helium cloud for each valve, marked as green dots in figure 1. Consequently, the measurement region starts close to the target at 8 mm and can extend into the confined plasma region. The diagnostic covers the region near the strike line for the low-iota configuration, whereas for high-iota configuration, it measures deeply in the TSR and in the private flux region. In the latter configuration, the diagnostic is ineffective due to the low density and temperature, which reduces helium excitation and its emissivity compared to the low-iota configuration by a factor of 4–10 near the target.

The in-vessel hardware of the helium beam system is available at three different toroidal locations: the lower divertor of module 3 $\phi = 131.7°$ (HEB_30), the upper divertor of module 5 $\phi = 300.3°$ (HEB_51), and the outer midplane of module 2 $\phi = 72.0°$. Figure 2 shows the positions in a 3D representation of W7-X. As the polychromator system is independent of the in-vessel system, it can be operated either individually or simultaneously in all three positions. The only limitation is that the available channels of the polychromator are limited to 32 LOS. This means that simultaneous measurement at two or three toroidal positions reduces the available radial resolution. The two divertor helium beams are installed at stellarator-symmetric positions. In standard configuration both beams view on the same magnetic island and they are magnetically connected. The same applies to the MPM. Figures 2 and 3 show the positions of the diagnostics, along with a connecting magnetic field line in 3D and 2D. In the first picture, the whole torus of W7-X with divertor plates (black) and the confined plasma (blue) is shown. The magnetic island, in which the three diagnostics can view in standard configuration, is marked in orange, and the measurement regions are plotted in red. The colour-coded line represents one common field line which makes four toroidal turns, with the colour representing the distance to its starting point at HEB_30, with dark colours for small distances and bright colours for large distances. The magnification of each diagnostic location on the right shows that these locations can be connected by the same field line. Figure 3 shows the same type of colour plot as figure 1 but with both HEB systems and the MPM. Here, the colour-coded dots represent the intersection of the selected field line with the poloidal planes of the diagnostics, with dark colours representing short distances from its starting point and bright colours representing long distances from its starting point. With this setup, the helium beam is magnetically connected to the MPM and thus enables the observation of fast processes along the same field line at three different toroidal positions.

2.1. Signal quality and helium puff requirements

Due to its higher temporal resolution compared to the existing system at W7-X [34], and the smaller optical fibre diameter of 140 µm compared to similar systems at AUG with 400 µm [24, 25], the new

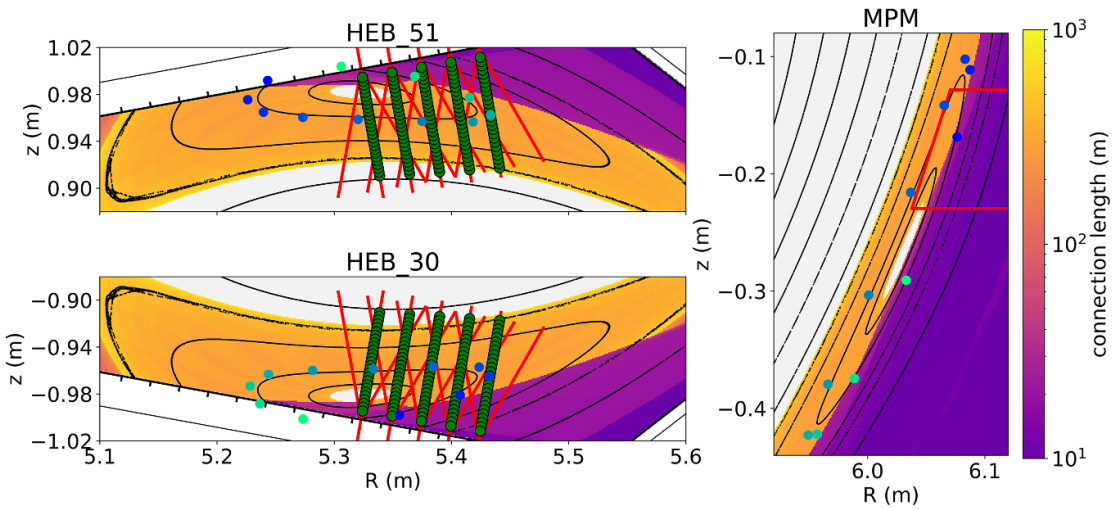

Figure 3. Schematic picture in standard configuration of the helium beam in the lower divertor of module 3 (HEB_30) and in the upper divertor of module 5 (HEB_51), as well as the MPM. The images correspond to figure 1, but the points where a field line crosses the plane have been added as colour-coded dots. Dark blue indicates the first point where the field line crosses, and green indicates the last point, before it approximately closes back on itself. Red lines in the right subplot indicate the measuring range of the MPM.

diagnostic requires a stronger diagnostic helium puff to achieve a comparable SNR. Without a higher diagnostic puff, the time resolution would have to be reduced to increase the SNR. Therefore, for high time-resolution measurements, a puff of 5×10^{19} atoms s^{-1} is used, which is 10 times higher than the standard puff for the existing helium beam system.

To investigate whether the increased helium puff perturbs the plasma, the response of global parameters to two diagnostic helium puffs is shown figure 4. For this particular investigation, the plasma pulse W7-X 20241121.046 in standard configuration is used alongside many others. In subfigure (a), the blue curve represents the ratio of a H^{I} and a He^{II} line, a proxy of the hydrogen to hydrogen plus helium ratio $n_H/(n_H + n_{He})$ [38]. Subfigure (b) combines two datasets: the absolute helium density near the magnetic axis obtained via charge exchange spectroscopy in orange, and in green the line-integrated electron density measured by interferometry [39, 40]. Subfigure (c) highlights the effective diagnostic helium puffs of valve number 4 in the divertor, which take 75 ms each time. In this plasma pulse only valve number 4 was used. For comparison with the helium puff, the corresponding signal of the fast helium beam diagnostic of the helium line 587.6 nm is shown in blue. Radiation levels, as captured by bolometers [41], are illustrated in subfigure (d), with outer, inner, and central LOS indicated by blue, orange, and green, respectively. Lastly, subfigure (e) compares the diamagnetic energy of the plasma (blue) [42] with the electron temperature from the outermost channel of the ECE diagnostic (orange) [43]. The dip at 11 s in (d) and (e) is due to lower ECRH power (green), not due to the puff. This figure demonstrates that no significant changes were observed in bolometers (d), the confined diamagnetic energy W_{dia} (e) and plasma temperature (e), suggesting that no global perturbation occurs. Nevertheless, a gradual accumulation of helium in the plasma is detected. Since helium is pumped slowly, it can be treated as a cumulative effect. For this plasma pulse, each puff raises the helium content by approximately 0.5%. The relative rise is mainly dependent on the plasma density. The accumulation limits the allowable puff number during a discharge.

The local impact of the diagnostic helium puff is assessed by comparing two identical plasma pulses, W7-X 20241127.014 and W7-X 20241127.022, in standard configuration, with line-integrated density of 3×10^{19} m^{-2} and ECRH input power of 2 MW. They differ only in the helium puff intensity, one with 5×10^{18} atoms s^{-1} and the other with 5×10^{19} atoms s^{-1}, puffed with valve 4. Density, pressure, and temperature profiles (in figures 5(a)–(c)) were reconstructed locally using the helium beam diagnostic itself. The temperature profiles were nearly identical, suggesting that no significant local cooling occurred as a result of the puff. However, a clear increase in the reconstructed density is observed. This increase does not indicate a real change in plasma conditions but is caused by reabsorption effects [23], which grow with higher helium densities and are not yet included in the currently used static model. This interpretation is supported by figures 5(d)–(f) where the measured intensities are shown. To take the different puffing strengths into account, the signals are normalised by their helium puff intensity. Here, the line emission profiles for 706 nm and 728 nm agree perfectly between the different puffing levels;

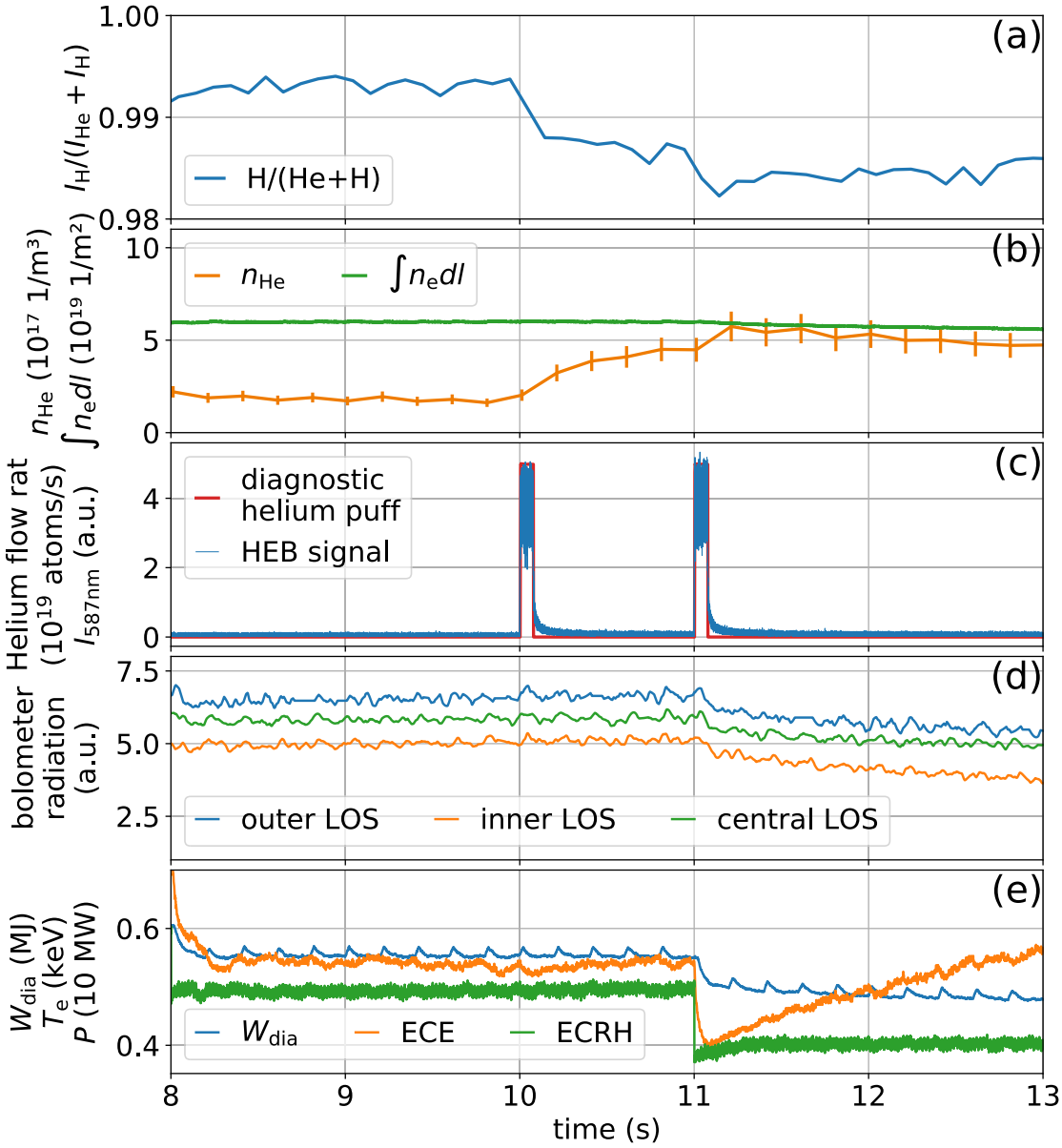

Figure 4. Overview of helium content and global plasma parameters during two diagnostic helium puffs of 5×10^{19} atoms s^{-1}, which correspond to the maximal puff level used. (a) The line emission intensity ratio of hydrogen to hydrogen plus helium at the plasma edge; (b) the absolute helium density near the magnetic axis measured via charge exchange spectroscopy in orange, line-integrated electron density obtained from interferometry in green; (c) the diagnostic helium puff in the divertor in red and the corresponding HEB signal of the 587.6 nm line with a time resolution of 10 µs in blue; (d) bolometer signals, with outer LOS in blue, inner LOS in orange, and central LOS in green; (e) diamagnetic energy of the plasma in blue, the electron temperature at the outermost channel of the ECE diagnostic in orange and the ECRH input power in green.

only the first channels $\leqslant$2 cm have slight deviations. For the 667 nm line, bigger discrepancies can be observed. This proves that there is indeed no electron density effect since the emissivity of every individual line is strongly density dependent, as given by

$$\epsilon = n_{He} n_e \mathrm{PEC}\,(n_e, T_e) \tag{1}$$

with ϵ the line emission, n_{He} the neutral helium density, n_e the electron density and PEC the photon emissivity coefficient. The reason for the observed changes of the 667 nm line emission lies in reabsorption and radiation trapping, which gets stronger for higher neutral helium densities. The hypothesis is bagged by the observation that the discrepancy decreases with increasing distance to the target where the neutral helium density is lower. The effect on the reconstructed electron density was already well studied at TCV [23], where the same effect of an increase in reconstructed density but not temperature was observed for similar gas puffs of 6×10^{19} atoms s^{-1}. This issue was resolved by taking reabsorption into

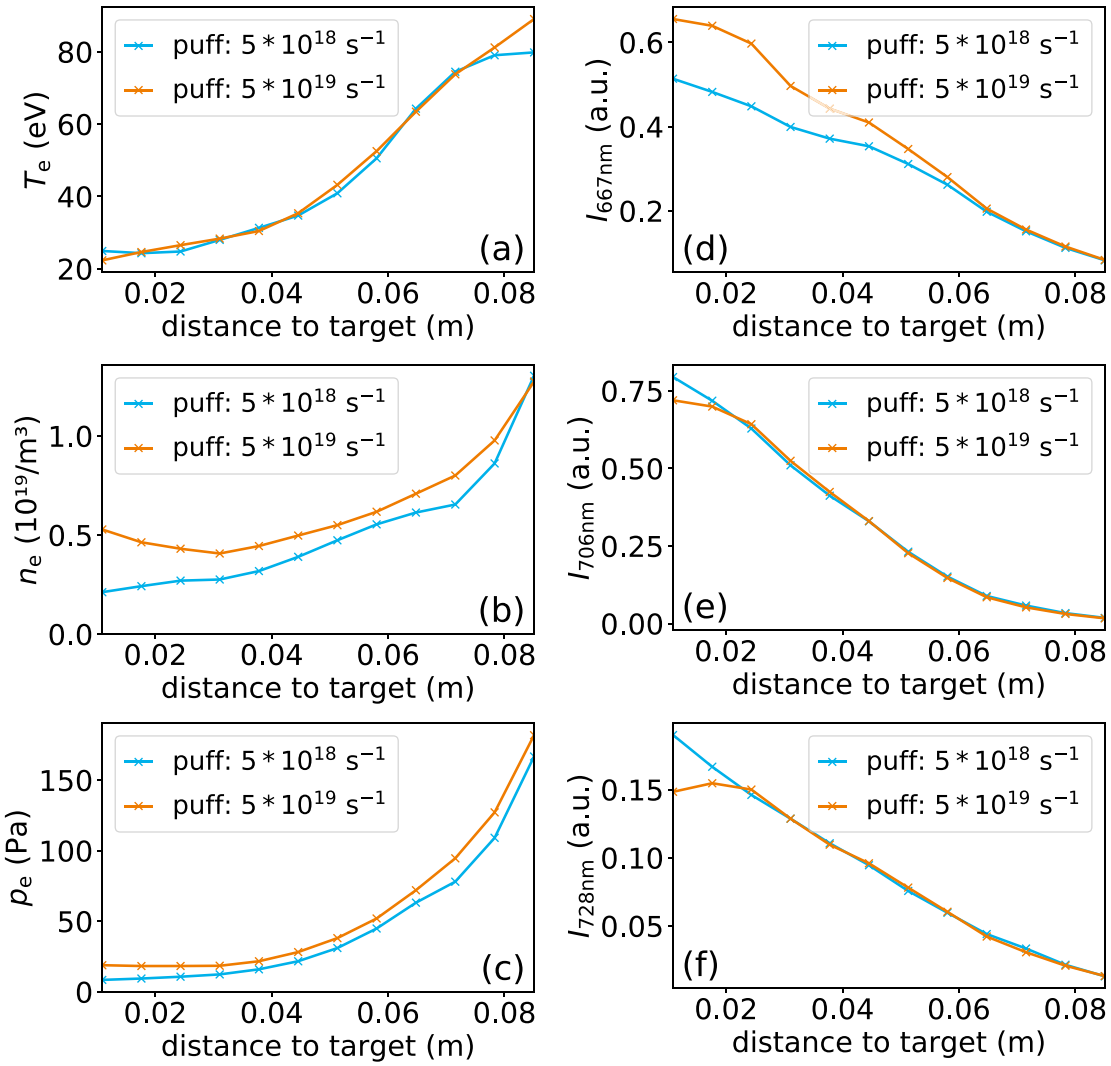

Figure 5. 1D electron temperature (a), density (b) and pressure (c) profiles measured by the helium beam and averaged over one diagnostic helium puff (75 ms). Two identical pulses W7-X 20241127.014 and W7-X 20241127.022 at 4.9 s with two different diagnostic helium puffs $\approx 5 \times 10^{18}$ atoms s^{-1} (blue) and $\approx 5 \times 10^{19}$ atoms s^{-1} (orange) are compared. The second column shows the intensities of the three helium lines at 667 nm (d), 706 nm (e) and 728 nm (f). For the intensities, the signals are normalised by their puffing strength.

the CRM [23, 44]. For future work, we plan to implement the dynamic model already used on AUG, which includes reabsorption, dynamic state-mixing and LOS integration [31]. This model is therefore one of several available methods to account for reabsorption. However, the simple evaluation using the static model should remain unchanged without reabsorption. This analysis concludes that the higher gas puff intensity of 5×10^{19} atoms s^{-1} does not perturb the plasma globally nor locally for target distances larger than 2 cm. Furthermore, it was found that, for higher gas puffs near the target, the density reconstruction by the static model is overestimated, and that a new CRM with reabsorption must be implemented to address this issue.

The SNR for 1 µs, 10 µs and 100 µs time resolution for all four wavelength is shown in figures 6(a)–(c), while the signal-to-background ratio (SBR) is illustrated in figure 6(d). For the SNR analysis, valve 4 in plasma pulse W7-X 20241127.027 is used. The plasma pulse is in standard configuration and has an integrated electron density of 8×10^{19} m^{-2} and an ECRH heating of 3 MW. The SNR is calculated using the autocorrelation of the signals, as described in [45]. With this method, noise appears as a sharp peak at zero time shift in the autocorrelation, while the signal is defined as the interpolated maximum of the broader correlation peak. This is because uncorrelated noise contributes only at perfect overlap, whereas plasma fluctuations exhibit a wider correlation structure. For the SBR analysis the background is determined by the averaged passive plasma emission without beam. From the figure 6, it can be seen that for 1 µs resolution, only the strongest helium line at 587 nm yields a sufficient SNR near the target. Consequently, to use line ratios, a time resolution of at least 10 µs is required near the target and several

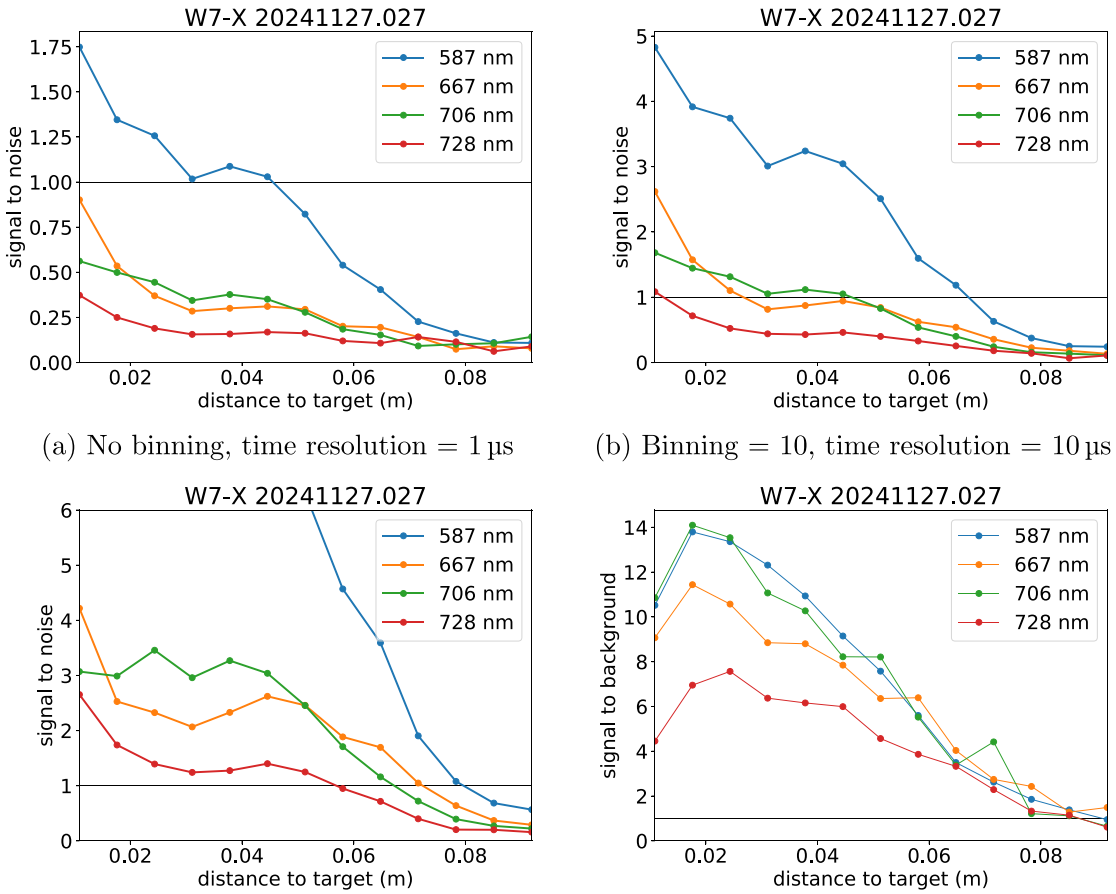

Figure 6. Signal-to-noise ratio (SNR) (a)–(c) for different time resolutions of the four investigated wavelengths for a standard discharge in standard configuration. (d) Shows the corresponding signal-to-background ratio. For the measurement, a diagnostic helium puff of 5×10^{19} atoms s^{-1} is used. The horizontal black line marks the threshold of 1. The SNR is calculated by using the autocorrelation of the signal.

10 µs for most of the island region. For accurate density and temperature calculations, where especially the weak 728 nm line is needed, a binning time of ≈100 µs is necessary. Furthermore, figure 6(d) shows a high SBR, proving that background plasma emission contributes minimally to the observed signal up to 7 cm above the target, which is required for localised measurements.

The resulting time resolution of 1D profiles of 1–10 µs for emission lines and a resolution of 100 µs for n_e and T_e in the divertor region makes this diagnostic unique at W7-X. Furthermore, it is also the first diagnostic for 1D edge temperature profiles with such high time resolution at W7-X.

2.2. Cross diagnostic comparison

The following subsection presents a comparison between the two helium beam systems. For this, plasma pulse W7-X 20241024.038 is used, which is in standard configuration. The diagnostic puff was created by valve 4. To match the time resolution of the spectrometer-based system (25 ms), 25 000 consecutive time points from the fast helium beam system were averaged. This averaging allows a direct comparison between the two diagnostics at the same temporal resolution. Furthermore, as both systems use the same optical components within the vessel, they measure at the same position. The result is shown in figure 7, where the blue curve represents the new system and the orange line the spectrometer system. For this comparison, both diagnostics used the same static CRM from [28] for reconstruction and the standard low-intensity puff from the existing system with 5×10^{18} atoms s^{-1} was used. Both systems exhibit excellent agreement in the reconstructed electron temperature (a) and pressure (c), with only minor deviations observed in the density profiles (b). The measured intensity profiles of both diagnostics agree almost completely ((d)–(f)), only the 667 nm helium line shows small deviations. This confirms that the new diagnostic can achieve a similar level of accuracy as the existing system. Moreover, the new system also enabled the reconstruction of a 2D profile using four separate puffs at different spatial locations, see figure 8. In this method, each valve is opened individually for 75 ms, and the background is

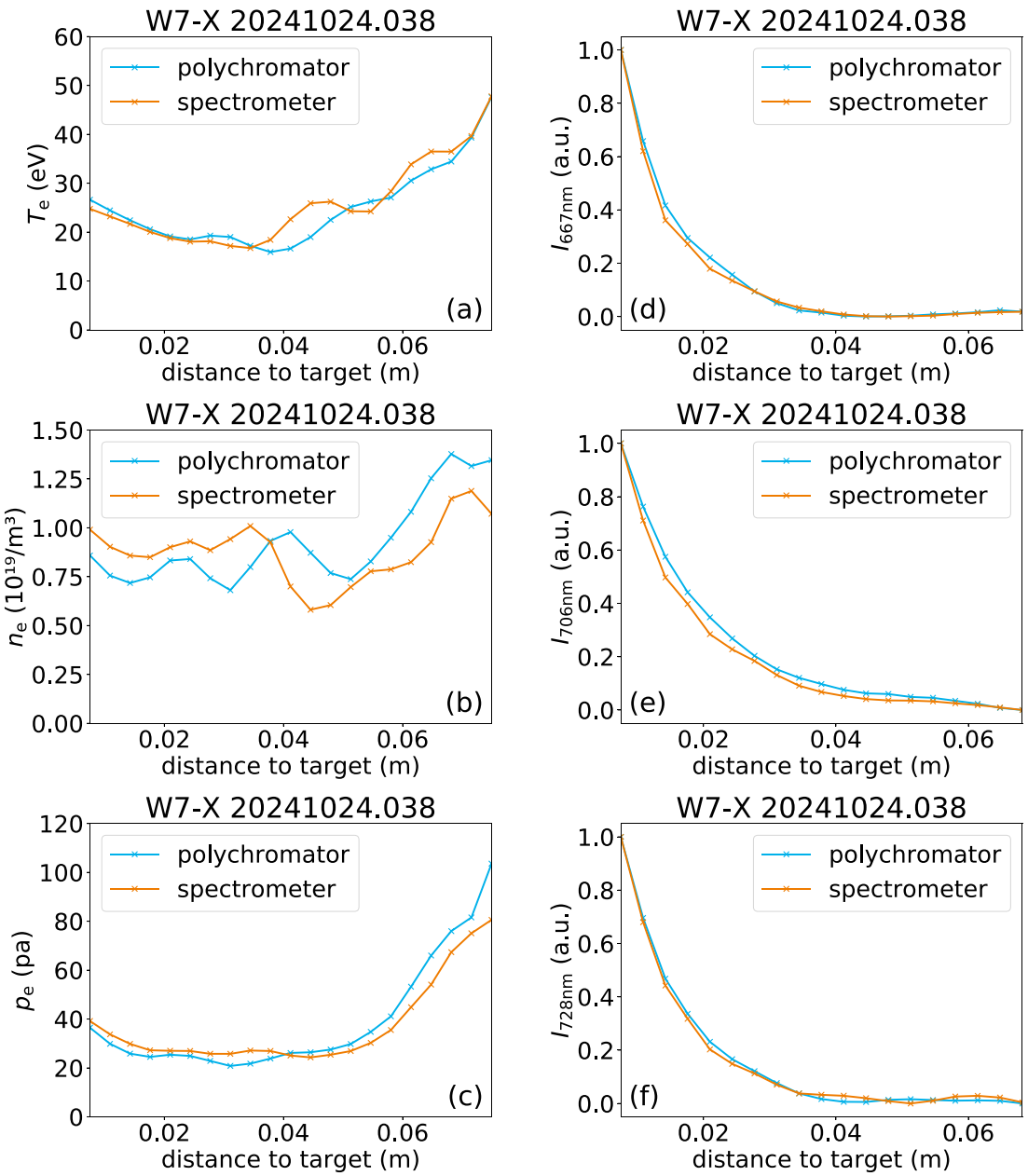

Figure 7. 1D electron temperature (a), density (b) and pressure (c) profile as well as the normalised and plasma background corrected intensity of the measured three helium lines (d)–(f) averaged over 25 ms. Here, the already existing helium beam system with spectrometers (orange) is compared with the new polychromator system (blue). Both datasets are analysed with the same collisional radiative model. These measurements were done with the standard low gas puff of 5×10^{18} atoms s^{-1}.

measured for 75 ms between puffs. The four 1D profiles generated in this way at different positions are then combined to form a 2D image. It is important that the plasma parameters remain constant during the entire 600 ms required for such a measurement. It should also be noted that this measurement allows a better resolution in z direction than in the R direction. This technique was already demonstrated in [34, 35].

3. Fast plasma dynamics in the island divertor

The new fast helium beam diagnostic is the first system at W7-X that enables the reconstruction of electron density and temperature profiles with high temporal resolution at the plasma edge. Additionally, it offers, for the first time, insights into the fast plasma dynamics in the divertor volume. Toroidal long-range correlation measurements can also be performed by using two magnetically coupled measuring points in different divertors. Each of these features should demonstrate the diagnostic potential and is

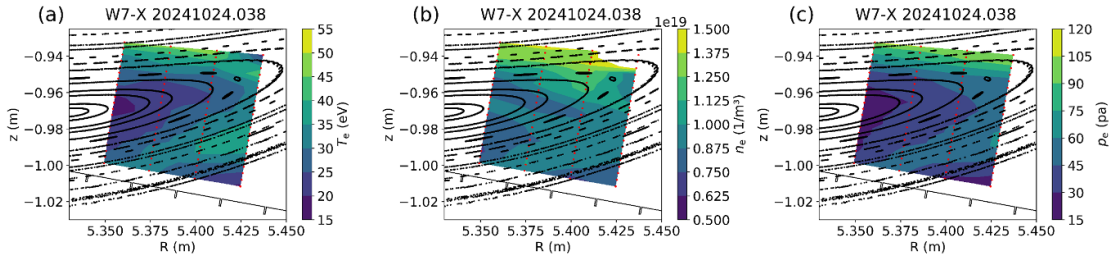

Figure 8. 2D profiles of (a) electron temperature, (b) electron density and (c) electron pressure taken by the polychromator system. A Poincaré plot is overlaid to show the magnetic island. Measurement points used for the reconstruction are marked in red. The procedure is based on the method of [34].

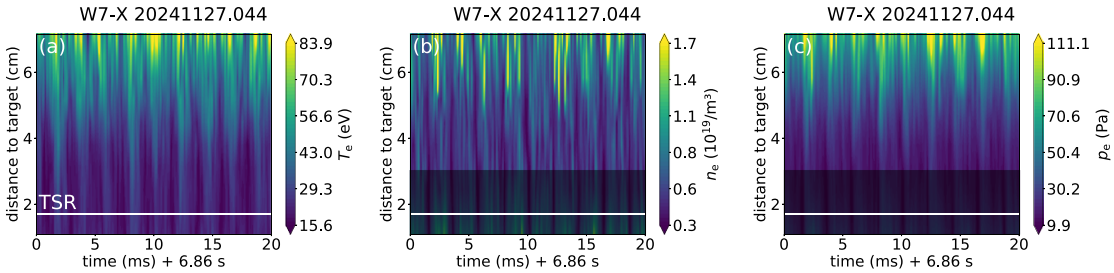

Figure 9. Electron temperature (a), electron density (b) and electron pressure profile (c) of the island region during the presence of a low frequency mode at 460 Hz. The measurement positions correspond to valve four near the O-point, see figure 1. The shadowed areas near the target in n_e and p_e represent the region where the used model overestimates the density and therefore also the pressure due to reabsorption and radiation trapping. The white line marks the target shadow region (TSR).

described individually below, with first measurement results. However, the analysis is not performed in depth.

3.1. Fast electron density and temperature profiles

Highly time-resolved radial electron temperature and density profiles can be achieved with a time resolution of up to 100 µs. An example is shown in figure 9. Here, plasma pulse W7-X 20241127.044 is analysed, which is a standard configuration with an line-integrated electron density of $3 \times 10^{19}\,\mathrm{m}^{-2}$ and an ECRH input power of 2 MW. In figure 9(a), the electron temperature, (b) the electron density, and (c) the electron pressure are shown. For this measurement, valve 4 with the strong diagnostic helium puff of 5×10^{19} atoms s^{-1} was used, and the data are binned to 300 µs.

As discussed in section 2.1, with the high puff intensity the electron density, and consequently also the pressure, near the target is overestimated due to reabsorption effects, which are not yet considered in the CRM used. Therefore, the regions which show deviation in n_e are shaded in the plots. The W7-X plasma pulse is subject to a low frequency $m = 1$ mode at 460 Hz. This mode has already been investigated in [46], and is known to be an intrinsic feature of the standard configuration.

In figure 9 this mode is visible and has a strong influence on both temperature and density, affecting regions near the target as well as within the island itself. Relative fluctuations of up to 50% are observed in both parameters. This highlights the importance of studying high-time-resolution profiles. Moreover, these measurements can provide valuable insights into the nature and transport effects of the mode. A more detailed discussion of the underlying physics of such low frequency modes in different configurations will be addressed in a future publication.

3.2. Long-range toroidal correlation measurement

Figures 2 and 3 demonstrate that both the upper and lower helium beam systems, as well as the MPM, are magnetically connected in standard configuration. This enables the investigation of long-range toroidal correlation measurements. To get a direct connection in one circumference between the upper and lower measurement locations, a valve close to the island centre has to be selected. This can be seen in figure 3 since the intersection points of the single field line marked by the colour-coded dots are mirrored around the island centre so that the field line generally needs several circumferences to intersect the observation volume of both HEB systems. However, by selecting valves near the mirroring axis, which is near the island centre, the same field line closes in under one circumference.

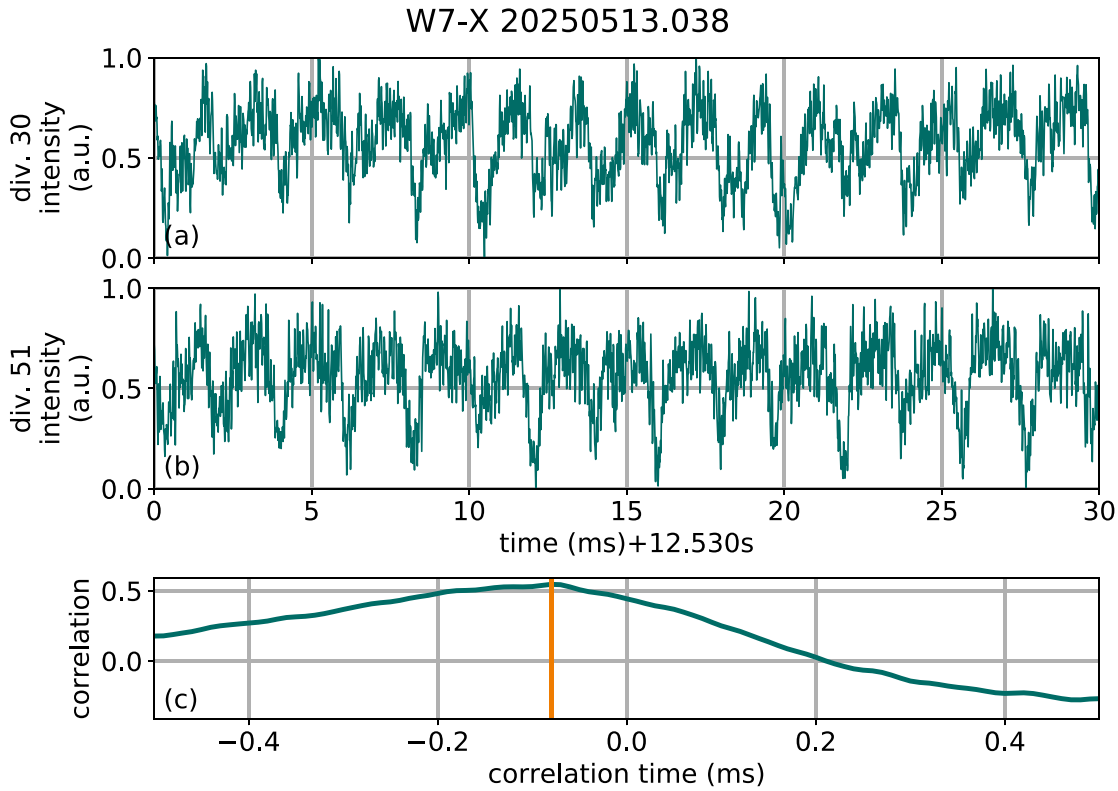

Figure 10. Figures (a) and (b) show the normalised raw signal of the 587 nm spectral line. The dynamic is dominated by the low frequency $m = 1$ mode. They are recorded at magnetically connected positions, in divertor 30 (a) and divertor 51 (b). (c) Shows the correlation of these signals, with its maximum marked in orange. The data are binned to a time resolution of 10 µs.

An example of such a toroidal correlation of normalised measurement signals is shown in figure 10. The used plasma pulse W7-X 20250513.038 is in the standard configuration with the same parameters as in section 3.1. Here, the signal in (a) originates from valve four of divertor 30 and (b) from valve five of divertor 51. According to field line tracing, both measurement points include the same magnetic field line in the integration volume. The dynamics of the emission intensities of the 587 nm line and also its correlation are dominated by the same low frequency m = 1 mode, as already shown in section 3.1. This analysis shows that on time scale of milliseconds, which is in the order of the frequency of the mode, the correlation exhibits a periodicity associated with the investigated mode. Furthermore, on small timescales, a slight time delay of 80 µs between the signals from the different divertors is observed. The negative time lag of the maximum of the correlation in figure 10(c) means that the signal of divertor 51 comes before the signal of divertor 30. As the correlation function is relatively flat on short time scales, the exact time offset has an uncertainty of several 10 µs. But this offset could be determined more accurately with the help of other channels.

However, a time offset that is not equal to zero can be confirmed. Since the mode originates from the outer core and propagates into the SOL [46], this time difference in signal propagation is a possible indication of a preferred toroidal entry point of the particles in the SOL. Another possible explanation for this is a preferred transport direction. Both possibilities will be analysed in the future. Moreover, this setup enables the determination of the toroidal mode numbers. In addition to toroidal correlation measurements, poloidal correlations can be obtained by comparing measurement points located on the same magnetic flux surface within a single divertor.

3.3. Detachment analysis

Another essential topic of divertor physics is divertor plasma detachment. This phenomenon describes a regime in which the heat and particle fluxes onto the divertor targets are reduced, while the volumetric energy dissipation, such as radiation, accounts for a large fraction of the power exhaust. Detachment is a key requirement for future fusion power plants, both for tokamaks such as ITER [47] and DEMO [48] and for stellarators [49], since the expected heat fluxes exceed the tolerances of current plasma-facing materials unless detachment occurs [50, 51]. This state is typically achieved by enhancing radiation losses, either through impurity seeding or by increasing the divertor plasma density [52].

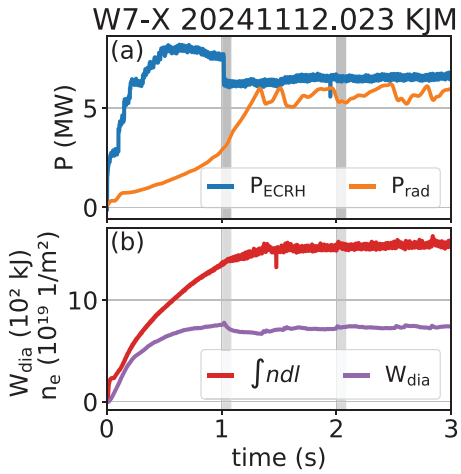

Figure 11. Plot (a) shows the ECRH power input in blue and the power radiated by the plasma in orange. The diamagnetic energy (purple) and line-integrated density measured by interferometers (red) are shown in (b). The grey areas show the sections where active helium was puffed in the divertor. The profiles generated from these are shown in figure 12.

Since the temperatures during detachment are too low to effectively excite helium, the helium beam diagnostic can only determine the density and temperature up to the onset of detachment. Therefore, this diagnostic will be used primarily to study the dynamics of detachment and the fast process during detachment via individual helium lines.

One diagnostic approach of the helium beam to investigate the physics of detachment is the line-integrated method, which relies on passive helium emission. This method takes advantage of the fact that each impurity line, due to the interplay of recombination and excitation, emits most strongly at a particular local combination of electron temperature and density. As a result, changes in emission profiles can be used to track the position and movement of the emission front. Since it does not require a diagnostic helium puff, this technique allows for continuous, non-invasive monitoring of the detachment state [53].

In contrast, local measurements can be achieved by using active helium injection. In the attached regime, the target temperature is high, producing strong helium line radiation near the divertor plates. However, due to high ionisation rates in this hot region, only a small fraction of neutral helium penetrates to the inner channels away from the target, leading to a weak signal level there. In the detached regime, the plasma near the target is much cooler, leading to weak or absent helium excitation and thus a low signal at the target itself. However, the lower ionisation rate also means that more neutral helium reaches further into the plasma, increasing the signal in the inner channels. This leads to a characteristic shift of the intensity maximum, moving from the divertor target during the attached phase to more inward regions during detachment [54]. The advantages of using an active helium puff to measure detachment are the higher signal and localised measurement.

A detachment process with an active helium puff was studied on plasma pulse W7-X 20241112.023 in high mirror configuration. Figure 11 shows the most important parameters: ECRH power (blue), radiated power (orange), line-integrated core electron density (red) and confined diamagnetic energy W_{dia} (purple). The puff phases of valve 4 of the helium beam are marked in grey, and the corresponding helium beam data are shown in figures 12(a) and (b). Figure 12(a) illustrates the signal during the detachment transition, and figure 12(b) shows the fully detached case. For this experiment, the low puff rate of 5×10^{18} atoms s^{-1} is sufficient to resolve detachment while not influencing the detachment process. The time resolution of both plots is 100 µs.

For the first time in W7-X, the high temporal resolution enables detailed analysis of the detachment process in 1D. It becomes evident that detachment in the high-mirror magnetic configuration is not a smooth, gradual transition but is punctuated by rapid intermittent events. These events are not only related to detachment but can have significant influence on it. In figures 12(a) and (b), these events become visible as vertical stripes, for example, at 1.055 s and 2.038 s. The intermittent events are particularly relevant because they exhibit locally increased temperature and density, potentially leading to enhanced sputtering at the divertor target. Due to the highly non-linear dependence of sputtering yields on ion temperature [7–9], these short-living events may dominate the overall erosion of plasma-facing components during detachment, despite contributing insignificantly to time-averaged profiles. It should be mentioned that only emissivity is shown here and not the ion temperature responsible for sputtering.

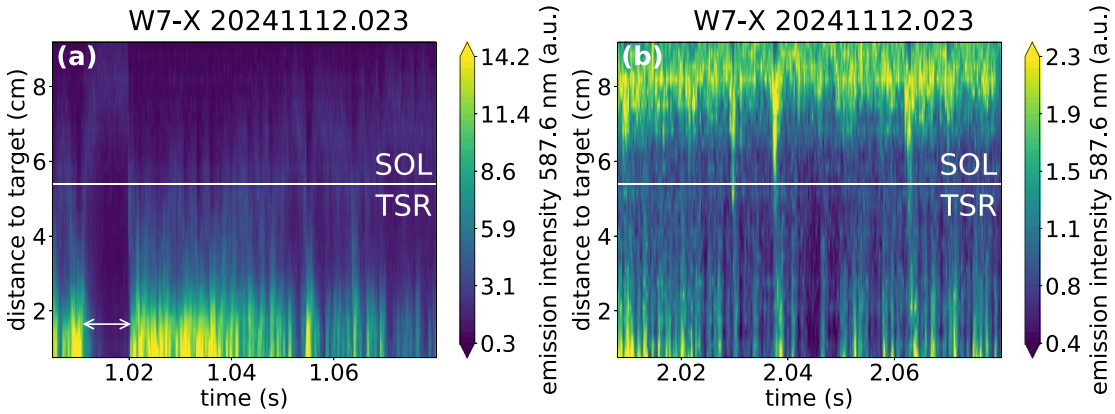

Figure 12. (a) shows a colour plot of the intensity of the 587 nm line during a detachment process. The normalisation was applied to each channel individually. The distance to the target is plotted on the y-axis. The entire phase is during a diagnostic helium puff of valve 4 with puffing rate 5×10^{18} atoms s^{-1}. The data are binned and smoothed to a time resolution of 100 µs. In (b), a similar plot is shown, but during a time range with complete detachment. Both periods are marked in figure 11 to put them in the context of the discharge. The white line shows the transition to the scrape-off layer (SOL) and target shadow region (TSR) while the white arrow shows the time width of the strong intermittent event.

Furthermore, it should also be mentioned that there is a steep drop in emissivity below a temperature of approximately 8 eV, and thus the effect could be smaller than it appears from intensity alone. For this reason, future detailed investigations involving also several different diagnostics are indispensable.

Additionally, a strong event was recorded (see figure 12(a)), time 1.0109–1.0204 s, marked by the white arrow) with extremely fast transition timescales; the back transition, for example, takes only 500 µs. At the moment, there is no validated explanation for such strong events with fast transitions. The only recognised pattern is that the back transition coincides with a partial loss of ECRH. One possible explanation could be a local detachment or a local or global turbulent event. Another explanation is that in this phase the divertor is in an oscillating detachment as already observed in tokamaks like JET [55] and AUG [56] and is explained for these machines by [57, 58]. This is supported by the observation that before 1.0109 s there is another strong but slightly smaller event. However, for each of these possible explanations, further observations are needed. These measurements suggest that the newly developed diagnostic system can offer significant insight into the dynamics and stability of detachment in the W7-X island divertor.

4. Conclusion and outlook

In summary, although W7-X already features extensive fast diagnostics, local fast measurements are lacking in the divertor region. This issue has been improved through the development of a fast helium beam system, which utilises the in-vessel components of the existing helium beam setup but employs an acquisition system based on PMTs, that is 25 000 times faster than the previous one. With this system a temporal resolution of up to 1 µs for intensity measurements and 100 µs for electron temperature (T_e) and density (n_e) measurements is achieved.

On the slow timescales, a direct comparison with the existing system demonstrated excellent agreement, confirming that the new diagnostic can reconstruct slow 2D profiles with high accuracy. Furthermore, it was found that the increased diagnostic helium puff required for the higher time resolution does not perturb the plasma, neither globally nor locally. However, the cumulative helium input increases the overall helium content, potentially reducing the available diagnostic measurement time in a given discharge. For a precise n_e determination near the target at high puffing rates, reabsorption effects need to be considered in the CRM.

As a demonstration of the diagnostic performance, experiments on three physical topics were briefly reported. The main potential of this diagnostic lies in its ability to provide fast measurements of T_e and n_e within the divertor volume. It also represents the first diagnostic at W7-X, providing fast 1D T_e profiles in the SOL. This opens up the possibility of investigating edge and divertor instabilities, modes, and fluctuations in unprecedented detail. Because the system is installed at three toroidally separated locations, two of which are magnetically connected divertors, it is now possible, for the first time, to measure at multiple toroidal positions using the same fast diagnostic. This makes it feasible to study toroidal asymmetries in fluctuations as well as long-range correlations. These studies enable the determination

of parallel velocities, wavenumbers, and potentially even characteristics of parallel transport. Lastly, the new system enables local, highly resolved investigations of the dynamics of the detachment process and the fast processes during detachment, by using a single emission line. Furthermore, strong intermittent events that are not yet fully understood were observed and characterised for the first time during detachment in W7-X with such detail.

Looking ahead, an upgrade to include toroidal LOS is envisioned, which would allow for fast 2D profiles with 100 µs time resolution. Additionally, larger-diameter fibres with a diameter of 400 µm, which are used at AUG, would increase the effective area in which light is collected and therefore the signal by a factor of eight. This eliminates the need for high gas puffs, which increases the signal by a factor of ten. In the meantime, embedding reabsorption effects in the CRM should solve the issue of overestimating the density near the wall. Furthermore, higher puffs are planned during the detachment to enhance the signal. In combination with another CRM, this could potentially enable the reconstruction of n_e and T_e deeper into the detachment.

In conclusion, the new fast helium beam diagnostic provides a unique and versatile tool that significantly expands the diagnostic capabilities of W7-X, filling a critical gap in divertor and edge measurements, and opening new ways for plasma edge physics.

Data availability statement

The data cannot be made publicly available upon publication because they are not available in a format that is sufficiently accessible or reusable by other researchers. The data that support the findings of this study are available upon reasonable request from the authors.

Acknowledgments

This work received funding from the German Federal Ministry of Research, Technology and Space (BMFTR) within the funding program Fusion 2040 (reference No. 13F1020).

This work has been carried out within the framework of the EUROfusion Consortium, funded by the European Union via the Euratom Research and Training Programme (Grant Agreement No 101052200 — EUROfusion). Views and opinions expressed are however those of the author(s) only and do not necessarily reflect those of the European Union or the European Commission. Neither the European Union nor the European Commission can be held responsible for them.

ORCID iDs

S Hörmann 0009-0004-5704-7114
M Griener 0000-0003-2953-536X
M Krychowiak 0009-0001-4141-5558
D Gradic 0000-0002-6109-9345
F B T Siddiki 0000-0002-0474-300X
M Astrain 0000-0003-3486-0941
E Flom 0000-0002-9284-9380
G Birkenmeier 0000-0001-7508-3646
A von Stechow 0000-0003-0277-4600
C Killer 0000-0001-7747-3066
F Reimold 0000-0003-4251-7924
S Sereda 0000-0003-0180-6279
T Romba 0000-0002-2727-9385
K J Brunner 0000-0002-0974-0457
J Knauer 0000-0001-7359-6472
U Stroth 0000-0003-1104-2233

References

[1] Renner H, Boscary J, Greuner H, Grote H, Hoffmann F W, Kisslinger J, Strumberger E and Mendelevitch B 2002 Divertor concept for the W7-X stellarator and mode of operation *Plasma Phys. Control. Fusion* **44** 1005
[2] König R *et al* 2002 The divertor program in stellarators *Plasma Phys. Control. Fusion* **44** 2365
[3] Grigull P *et al* (The W7-AS Team) 2001 First island divertor experiments on the W7-AS stellarator *Plasma Phys. Control. Fusion* **43** A175
[4] Maaziz N, Reimold F, Winters V, Bold D, Feng Y and Perseo V 2025 Investigating the role of divertor geometry on density build-up in the island divertor *Nucl. Mater. Energy* **42** 101886

[5] Feng Y, Sardei F, Grigull P, McCormick K, Kisslinger J and Reiter D 2006 Physics of island divertors as highlighted by the example of W7-AS *Nucl. Fusion* **46** 807
[6] Feng Y, Kobayashi M, Lunt T and Reiter D 2011 Comparison between stellarator and tokamak divertor transport *Plasma Phys. Control. Fusion* **53** 024009
[7] Birkenmeier G *et al* 2015 Filament transport, warm ions and erosion in ASDEX upgrade L-modes *Nucl. Fusion* **55** 033018
[8] Brezinsek S 2015 Plasma-surface interaction in the Be/W environment: conclusions drawn from the JET-ILW for ITER *J. Nucl. Mater.* **463** 11–21
[9] Redl A *et al* (The ASDEX Upgrade Team and the EUROfusion Tokamak Exploitation Team) 2024 An extensive analysis of SOL properties in high-δ plasmas in ASDEX upgrade *Nucl. Fusion* **64** 086064
[10] Griener M *et al* 2020 Continuous observation of filaments from the confined region to the far scrape-off layer *Nucl. Mater. Energy* **25** 100854
[11] Stagni A *et al* 2024 The effect of plasma shaping on high density H-mode SOL profiles and fluctuations in TCV *Nucl. Fusion* **64** 026016
[12] Perillo R, Boedo J A, Lasnier C J, McLean A, Bykov I, Marini C, Rudakov D L and Watkins J G (DIII-D Team) 2024 Experimental evidence of enhanced radial transport in small ELM regimes at DIII-D *Phys. Plasmas* **31** 022503
[13] Killer C, Shanahan B, Grulke O, Endler M, Hammond K and Rudischhauser L (W7-X Team) 2020 Plasma filaments in the scrape-off layer of Wendelstein 7-X *Plasma Phys. Control. Fusion* **62** 085003
[14] Terry J L *et al* 2024 Realization of a gas puff imaging system on the Wendelstein 7-X stellarator *Rev. Sci. Instrum.* **95** 093517
[15] Baek S, Ballinger S, Grulke O, Killer C, von Stechow A, Terry J, Scharmer F and Shanahan B 2025 Gas puff imaging of plasma turbulence in the magnetic island scrape-off layer of W7-X *Nucl. Mater. Energy* **43** 101937
[16] Killer C, Drews P, Grulke O, Knieps A, Nicolai D and Satheeswaran G (on behalf of the W7-X Team) 2022 Reciprocating probe measurements in the test divertor operation phase of Wendelstein 7-X *J. Instrum.* **17** 03018
[17] Killer C, Cipciar D, Baek S G, Ballinger S B, v. Stechow A, Terry J L and Grulke O (The W7-X Team) 2025 Electric fields and stationary drift flows in the island divertor SOL of Wendelstein 7-X *Nucl. Fusion* **65** 056026
[18] Pandey A *et al* 2024 Pop-up Langmuir probe diagnostic in the water cooled divertor of Wendelstein 7-X *Rev. Sci. Instrum.* **95** 043503
[19] Anda G, Dunai D, Krizsanóczi T, Nagy D, Otte M, Hegedüs S, Vécsei M, Zoletnik S and Gárdonyi G 2019 Measurement of edge plasma parameters at W7-X using alkali beam emission spectroscopy *Fusion Eng. Des.* **146** 1814–9
[20] Vécsei M, Anda G, Asztalos O, Dunai D, Hegedüs S, Nagy D, Otte M, Pokol G I, Zoletnik S and Team W-X 2021 Swift evaluation of electron density profiles obtained by the alkali beam emission spectroscopy technique using linearized reconstruction *Rev. Sci. Instrum.* **92** 113501
[21] Jones O *et al* 2016 Development of a thermal helium beam emission diagnostic for west *43rd EPS Conf. Plasma Physics* (available at: ocs.ciemat.es/EPS2016PAP/pdf/P5.022.pdf) pp 1–4
[22] Schmitz O *et al* (The TEXTOR team) 2008 Status of electron temperature and density measurement with beam emission spectroscopy on thermal helium at textor *Plasma Phys. Control. Fusion* **50** 115004
[23] Ugoletti M *et al* 2024 Role of radiation re-absorption in the thermal helium beam diagnostic *Rev. Sci. Instrum.* **95** 083530
[24] Griener M, Wolfrum E, Cavedon M, Dux R, Rohde V, Sochor M, Muñoz Burgos J M, Schmitz O and Stroth U 2018 Helium line ratio spectroscopy for high spatiotemporal resolution plasma edge profile measurements at ASDEX upgrade (invited) *Rev. Sci. Instrum.* **89** 10D102
[25] Hörmann S *et al* 2024 Thermal helium beam diagnostic for 2D profile measurements in the divertor of ASDEX upgrade *Rev. Sci. Instrum.* **95** 113507
[26] Agostini M, Scarin P, Cavazzana R, Carraro L, Grando L, Taliercio C, Franchin L and Tiso A 2015 Fast thermal helium beam diagnostic for measurements of edge electron profiles and fluctuations *Rev. Sci. Instrum.* **86** 123513
[27] Davies S *et al* 1997 Parallel electron temperature and density gradients measured in the JET mki divertor using thermal helium beams *J. Nucl. Mater.* **241-243** 426–32
[28] Muñoz Burgos J M, Schmitz O, Loch S D and Ballance C P 2012 Hybrid time dependent/independent solution for the He I line ratio temperature and density diagnostic for a thermal helium beam with applications in the scrape-off layer-edge regions in tokamaks *Phys. Plasmas* **19** 012501
[29] Griener M *et al* 2017 Qualification and implementation of line ratio spectroscopy on helium as plasma edge diagnostic at ASDEX upgrade *Plasma Phys. Control. Fusion* **60** 025008
[30] Summers H P 2004 Atomic data and analysis structure user manual, (version 2.7 ed.) Atomic Data and Analysis Structure (available at: www.adas.ac.uk)
[31] Wendler D, Dux R, Fischer R, Griener M, Wolfrum E, Birkenmeier G and Stroth U 2022 Collisional radiative model for the evaluation of the thermal helium beam diagnostic at ASDEX upgrade *Plasma Phys. Control. Fusion* **64** 045004
[32] Griener M *et al* 2017 Fast piezoelectric valve offering controlled gas injection in magnetically confined fusion plasmas for diagnostic and fuelling purposes *Rev. Sci. Instrum.* **88** 033509
[33] Barbui T *et al* 2019 The He/Ne beam diagnostic for line-ratio spectroscopy in the island divertor of Wendelstein 7-X *J. Instrum.* **14** C07014
[34] Barbui T *et al* 2020 Measurements of plasma parameters in the divertor island of Wendelstein 7-X through line-ratio spectroscopy on helium *Nucl. Fusion* **60** 106014
[35] Flom E *et al* (the W7-X Team) 2023 Observation of a drift-driven local transport regime in the island divertor of Wendelstein 7-X (arXiv:2312.01240)
[36] Geiger J, Beidler C D, Feng Y, Maaßberg H, Marushchenko N B and Turkin Y 2014 Physics in the magnetic configuration space of W7-X *Plasma Phys. Control. Fusion* **57** 014004
[37] Klinger T *et al* 2019 Overview of first Wendelstein 7-X high-performance operation *Nucl. Fusion* **59** 112004
[38] Ford O P *et al* (W.-X. Team) 2024 Visible core spectroscopy at Wendelstein 7-X *Rev. Sci. Instrum.* **95** 083526
[39] Brunner K, Akiyama T, Hirsch M, Knauer J, Kornejew P, Kursinski B, Laqua H, Meineke J, Trimiño Mora H and Wolf R C 2018 Real-time dispersion interferometry for density feedback in fusion devices *J. Instrum.* **13** 09002
[40] Brunner K J, Knauer J, Meineke J, Castillo H I C, Hirsch M, Kursinski B, Stern M and Wolf R C (W7-X Team) 2022 Sources for constellation errors in modulated dispersion interferometers *Rev. Sci. Instrum.* **93** 023506
[41] Zhang D *et al* (the W7-X Team) 2021 Bolometer tomography on Wendelstein 7-X for study of radiation asymmetry *Nucl. Fusion* **61** 116043

[42] Rahbarnia K et al (the W7-X Team) 2018 Diamagnetic energy measurement during the first operational phase at the Wendelstein 7-X stellarator Nucl. Fusion 58 096010
[43] Hirsch M et al (The W7-X Team) 2019 ECE diagnostic for the initial operation of Wendelstein 7-X EPJ Web Conf. 203 03007
[44] Offeddu N et al 2022 Gas puff imaging on the TCV tokamak Rev. Sci. Instrum. 93 123504
[45] Zoletnik S, Fiedler S, Kocsis G, McCormick G K, Schweinzer J and Winter H P 1998 Determination of electron density fluctuation correlation functions via beam emission spectroscopy Plasma Phys. Control. Fusion 40 1399
[46] Cipciar D et al (The W7-X Team) 2025 Low frequency m = 1 modes during standard and improved confinement scenarios in W7-X Nucl. Fusion 65 046010
[47] Pitts R et al 2019 Physics basis for the first ITER tungsten divertor Nucl. Mater. Energy 20 100696
[48] Federici G, Biel W, Gilbert M, Kemp R, Taylor N and Wenninger R 2017 European demo design strategy and consequences for materials Nucl. Fusion 57 092002
[49] Feng Y 2013 Up-scaling the island divertor along the W7-stellarator line J. Nucl. Mater. 438 S497–500
[50] Pitts R et al 2017 Physics conclusions in support of ITER W divertor monoblock shaping Nucl. Mater. Energy 12 60–74
[51] Escourbiac F, Durocher A, Fedosov A, Hirai T, Pitts R, Gavila P, Riccardi B, Kuznetcov V, Volodin A and Komarov A 2019 Assessment of critical heat flux margins on tungsten monoblocks of the ITER divertor vertical targets Fusion Eng. Des. 146 2036–9
[52] Feng Y, Beidler C, Geiger J, Helander P, Hölbe H, Maassberg H, Turkin Y and Reiter D (W7-X Team) 2016 On the W7-X divertor performance under detached conditions Nucl. Fusion 56 126011
[53] Henke F 2025 Development and experimental validation of impurity line ratio spectroscopy for divertor plasmas at W7-X PhD Dissertation Universität Greifswald
[54] Hörmann S, Cavedon M, Griener M, Wendler D, Brida D, Wolfrum E and Stroth U (The ASDEX Upgrade Team) 2025 Two-dimensional dynamics of divertor detachment at ASDEX upgrade Plasma Phys. Control. Fusion 67 075016
[55] Loarte A, Monk R D, Kukushkin A S, Righi E, Campbell D J, Conway G D and Maggi C F 1999 Self-sustained divertor plasma oscillations in the JET tokamak Phys. Rev. Lett. 83 3657–60
[56] Heinrich P et al 2020 Self-sustained divertor oscillations in ASDEX upgrade Nucl. Fusion 60 076013
[57] Krasheninnikov S, Kukushkin A, Pistunovich V and Pozharov V 1987 Self-sustained oscillations in the divertor plasma Nucl. Fusion 27 1805
[58] Kukushkin A S and Krasheninnikov S I 2019 Bifurcations and oscillations in divertor plasma Plasma Phys. Control. Fusion 61 074001